PHYSICAL REVIEW D **91,** 114010 (2015)

Probing the top-quark chromomagnetic dipole moment at next-to-leading order in QCD

Diogo Buarque Franzosi[1,*] and Cen Zhang[2,†]

[1]*CP3-Origins, University of Southern Denmark, Campusvej 55, DK-5230 Odense M, Denmark*
[2]*Department of Physics, Brookhaven National Laboratory, Upton, New York 11973, USA*

(Received 14 April 2015; published 8 June 2015)

We present predictions at next-to-leading order (NLO) accuracy in QCD for top-quark pair production induced by an anomalous chromomagnetic dipole moment of the top quark. Our results are obtained for total as well as fully differential cross sections, including matching to parton shower simulations. This process is expected to provide the most stringent direct limits on top-quark chromomagnetic dipole moment. We find that NLO corrections increase the contribution from the dipole moment by about 50% at the LHC, and significantly reduce the renormalization and factorization scale dependence. Using the NLO prediction, we update the current limit from the Tevatron and the LHC measurements. Apart from total cross section, we also study other observables relevant for LHC phenomenology.

DOI: 10.1103/PhysRevD.91.114010 PACS numbers: 12.38.Bx, 14.65.Ha, 14.80.Bn

I. INTRODUCTION

The top quark is expected to play an important role in new physics searches, due to its large mass and strong coupling to the electroweak sector. Strategies to search for new physics effects in the top sector can be broadly divided into two categories. In the first category, we search for new resonant states, such as $t\bar{t}$ resonance and top partners. In the second category, new states are assumed to be too heavy to be directly produced, and their indirect effects are searched for in top-quark couplings.

Currently, no new states have been discovered, and exclusion limits have been placed, up to around several TeV scale for many new particles in either complete or simplified models [1]. On the other hand, in the second case the interaction of the top quark is becoming an ideal probe to new physics. On the experimental side, the millions of top quarks already produced at the LHC together with the tens of millions expected in the coming years will move top physics to a precision era. Many detailed and accurate information on various top-quark properties have been collected, and more will come. On the theory side, accurate standard model (SM) predictions are also available, in general at next-to-next-to-leading order (NNLO) in QCD and next-to-leading order (NLO) in electroweak for inclusive observables and at NLO in QCD for more exclusive ones. All of these provide the opportunity to extract or to constrain different anomalous top-quark couplings. In this context, theoretical predictions including QCD radiative corrections to anomalous top-quark couplings will be necessary for extracting precise and reliable limits, as leading order (LO) predictions in hadron colliders are often not reliable and suffer from large scale uncertainties. This has motivated a significant activity dedicated to providing the NLO QCD corrections to top-quark processes involving anomalous couplings, or higher-dimension operators [2–15]. However, NLO predictions involving anomalous top-quark interactions are still far from complete.

In this work we focus on the chromomagnetic dipole moment (CMDM) of the top quark in $t\bar{t}$ production. The cross section of $t\bar{t}$ production is one of the most accurately measured observables in top physics, and the effect of an anomalous CMDM has been investigated in many studies [16–29]. To the best of our knowledge, the contribution of top CMDM is known only at LO. The goal of this work is to promote it to NLO including fully differential productions and matching to parton showers, and investigate its impact on the current limits of top-quark CMDM, as well as other observables, with either stable or decayed $t\bar{t}$ system. We shall mention that, apart from CMDM, the top quark can also have an anomalous chromoelectric dipole moment (CEDM), which in this work we will not discuss. The reasons will be explained in the next section.

At first glance, one might expect deviations induced by anomalous top CMDM to be small, and therefore radiative corrections of these contributions to be a higher-order effect. However, in $t\bar{t}$ production at the LHC, the K factor from NLO QCD corrections is about 1.5 in the SM, and is numerically not a higher-order effect. If a similar K factor applies to the CMDM contribution, it will be important to know the NLO correction to the CMDM, so that a more accurate and stringent limit can be obtained. Moreover, this statement is too naive, since the issue is both on the accuracy, i.e. the central value, and on the precision, i.e. the uncertainties of a prediction. LO predictions for processes at Hadron colliders always suffer from large uncertainties due to scale variation, and the NLO predictions are expected to significantly reduce these uncertainties and

*franzosi@cp3-origins.net
†cenzhang@bnl.gov

thus provide a more reliable estimation of the possible range of the anomalous CMDM. Finally, in many cases NLO corrections can have an impact on kinematic distributions. Knowing the accurate differential cross section from the CMDM is therefore important in measurements where the shapes of the distributions are used. We will show such examples, where LO prediction for the distributions does not provide a reliable description.

The paper is organized as follows. In Sec. II we briefly discuss the theoretical background of top CMDM. In Sec. III we describe the framework of our calculation and how it is implemented. Our results for total cross sections and limits are presented in Sec. IV. In Sec. V we show several examples of exclusive distributions. Section VI is our conclusion.

II. THEORETICAL BACKGROUND

The top-quark chromomagnetic and chromoelectric dipole moments, CMDM and CEDM, can be parametrized by adding an effective term to the top-gluon coupling:

$$\mathcal{L}_{tt g} = g_s \bar{t}\gamma^\mu T^A t G^A_\mu + \frac{g_s}{m_t}\bar{t}\sigma^{\mu\nu}(d_V + i d_A \gamma_5) T^A t G^A_{\mu\nu} \quad (1)$$

where g_s is the strong coupling, and $G^A_{\mu\nu}$ is the gluon field strength tensor. d_V and d_A in the second term represent the CMDM and CEDM of the top quark respectively.

The CMDM of the top quark can arise from various models of new physics. The Yukawa corrections to $gt\bar{t}$ vertex in two Higgs doublet model (2HDM) was first considered in Ref. [16], while the supersymmetric QCD and electroweak corrections have been studied in Refs. [17–19]. Explicit expressions for CMDM in 2HDM and in minimal supersymmetric standard model were given in Ref. [20]. The top CMDM also arises quite naturally in composite models and technicolor models [21]. For a more general discussion of top CMDM in new physics scenarios we refer to Ref. [22]. Finally, a top CMDM operator may be loop induced by operator mixing effects, from other higher-dimensional operators generated at higher scales. An example can be found in Ref. [30].

Although processes like single top quark production [31] and Higgs boson production [32] and decay to jets [33] may contribute to access the CMDM at the LHC and Tevatron, the main constrain comes from $t\bar{t}$ production. Direct limits have been derived by previous studies [23–29,34,35]. However, the contribution of top CMDM has been known only at LO accuracy. Our aim is to provide the NLO prediction, as well as to study its impact on the total cross section and various distributions.

To go beyond LO calculation, a theoretical framework based on the dimension-six Lagrangian of the SM is required. This framework contains a complete set of operators satisfying the symmetries of the SM, i.e. the Lorentz symmetry and the $SU(3)_C \times SU(2)_L \times U(1)_Y$ gauge symmetries. It provides an unambiguous prescription for operator renormalization, and thus allows for a complete and consistent treatment of the higher-order corrections to the operators. The Lagrangian including dimension-six operators can be written as

$$\mathcal{L}_{\rm EFT} = \mathcal{L}_{\rm SM} + \sum_i \frac{C_i O_i}{\Lambda^2} + \text{H.c.} \quad (2)$$

where Λ is the scale of new physics. In this work we work up to order $\mathcal{O}(\Lambda^{-2})$, as going beyond this order would require complete knowledge of dimension-eight operators.

The top-quark CMDM in this framework is represented by a dimension-six operator

$$O_{tG} = y_t g_s (\bar{Q}\sigma^{\mu\nu} T^A t)\tilde{\phi} G^A_{\mu\nu}, \quad (3)$$

where Q is the left-handed top- and bottom-quark doublet, t the right-handed top, ϕ the Higgs doublet, and y_t the Yukawa coupling of the top quark. $\tilde{\phi} = i\sigma^2\phi^*$. This operator, after the electroweak symmetry breaking, takes the form of the second term in Eq. (1). The relation between d_V and the real part of the coefficient of O_{tG} is given by

$$d_V = \frac{\text{Re}C_{tG} m_t^2}{\Lambda^2}. \quad (4)$$

The operator O_{tG} contributes to $t\bar{t}$ production at tree level by modifying the standard $gt\bar{t}$ vertex, as well as inducing a new $ggt\bar{t}$ vertex, as shown in Fig. 1. The effects of this operator in top-quark processes at LO in QCD have been discussed in Refs. [36,37].

On the other hand, d_A, the CEDM, corresponds to the imaginary part of C_{tG}. In this work, however, we are going to focus only on the CMDM. This is because the analysis of the CEDM at NLO follows a completely different approach. As we have mentioned above, in an approach based on the dimension-six Lagrangian, we can only work up to order $\mathcal{O}(\Lambda^{-2})$, and thus only the interference between the CEDM and the SM amplitudes can be included. At this order the contribution vanishes in $t\bar{t}$ process because of the CP-odd nature of the CEDM, unless one incorporates the decay of the top quarks. As we shall see, our work is based on the MadGraph5_aMC@NLO framework [38], where the spin correlation and the off-shellness of the top-quark pairs are simulated by using the MadSpin package [39],

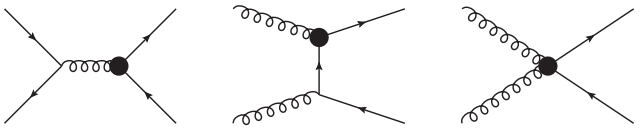

FIG. 1. Representative tree-level diagrams of $t\bar{t}$ production with an effective vertex form the operator O_{tG}. Black dot represents effective vertex from O_{tG}.

which is based on LO evaluation of the complete matrix element including top decays. Therefore it is not a suitable framework for the NLO corrections to the CP-odd effects of the CEDM, and we will leave the NLO analysis of the CEDM to future works. Throughout the paper, we assume C_{tG} to be real.

When going to NLO in QCD, one needs to take into account the operator mixing effects between O_{tG} and other dimension-six operators that could give a contribution to the same process at tree level. For $t\bar{t}$ production, these operators are $O_G = g_s f^{ABC} G_\mu^{A\nu} G_\nu^{B\rho} G_\rho^{C\mu}$, $O_{\phi G} = g_s^2 (\phi^\dagger \phi) G_{\mu\nu}^A G^{A\mu\nu}$, and several four-fermion operators [36]. It turns out that in $t\bar{t}$ production, the mixing from O_{tG} to these operators is not relevant. First of all, O_{tG} does not mix into O_G and four-fermion operators [30], because O_{tG} is essentially a dimension-five operator if the Higgs field always takes the vacuum expectation value, which is always true at the order we are working at. Second, O_{tG} does mix into $O_{\phi G}$ [32], but such effects correspond to a $\mathcal{O}(y_t^2)$ correction to the LO process, and therefore of higher order. Finally, the operators $O_{\phi G}$ and O_G do mix into O_{tG} [40], however it is consistent to assume that they vanish at all scales, given that they are not renormalized by O_{tG}. Therefore, as a first step, in this work we assume O_{tG} is the only nonvanishing operator, and neglect other operators. Note, however, that for a fully consistent phenomenological study, the complete operator set must be included. A first example of the global approach was presented for the flavor-changing neutral interactions of the top quark [41]. The NLO predictions for other operators will be left to future works.

III. FRAMEWORK AND IMPLEMENTATION

In a NLO calculation one has to choose a renormalization scheme. Our scheme is consistent with Ref. [6]. For the SM part, we adopt $\overline{\text{MS}}$ with five-flavor running in α_s with the top quark subtracted at zero-momentum transfer [42]. The bottom-quark mass is neglected. Masses and wave functions are renormalized on shell. The dimension-six operator O_{tG} then gives additional contributions to top-quark and gluon fields renormalization, as shown in Fig. 2. We find

$$\delta Z_2^{(t)} = \delta Z_{2,\text{SM}}^{(t)} - C_{tG} \frac{2\alpha_s m_t^2}{\pi\Lambda^2} D_\varepsilon \left(\frac{1}{\varepsilon_{UV}} + \frac{1}{3} \right) \tag{5}$$

FIG. 2. Contribution of O_{tG} operator to top-quark and gluon wave functions. Black dot represents effective vertex from O_{tG}.

$$\delta m_t = \delta m_{t,\text{SM}} - C_{tG} \frac{4\alpha_s m_t^3}{\pi\Lambda^2} D_\varepsilon \left(\frac{1}{\varepsilon_{UV}} + \frac{1}{3} \right) \tag{6}$$

$$\delta Z_2^{(g)} = \delta Z_{2,\text{SM}}^{(g)} - C_{tG} \frac{2\alpha_s m_t^2}{\pi\Lambda^2} D_\varepsilon \frac{1}{\varepsilon_{UV}}, \tag{7}$$

where

$$D_\varepsilon \equiv \Gamma(1+\varepsilon) \left(\frac{4\pi\mu^2}{m_t^2} \right)^\varepsilon, \tag{8}$$

and μ is the renormalization scale. In addition, the strong coupling counterterm, Z_{g_s}, also gets a dimension-six contribution:

$$\delta Z_{g_s} = \delta Z_{g_s,\text{SM}} + C_{tG} \frac{\alpha_s m_t^2}{\pi\Lambda^2} D_\varepsilon \frac{1}{\varepsilon_{UV}}, \tag{9}$$

that is to say the top-loop contribution with the operator O_{tG} is also decoupled from the running of α_s, in the same way as in the SM. Finally, for operator coefficient we use $\overline{\text{MS}}$ subtraction. The counterterm of C_{tG} is

$$\delta Z_{C_{tG}} = \frac{\alpha_s}{6\pi} \Gamma(1+\varepsilon)(4\pi)^\varepsilon. \tag{10}$$

This will lead to the running of C_{tG}.

One remark on Eq. (6) is in order. Naively if $\overline{\text{MS}}$ is applied to the complete set of dimension-six operators, one would expect that the dimension-six "Yukawa" operator, $O_{t\phi} = y_t^3 (\phi^\dagger \phi)(\bar{Q} t)\tilde{\phi}$, will be renormalized by O_{tG} and will be providing the UV pole in the mass counterterm in Eq. (6). The remaining finite term, however, still needs to be subtracted by introducing the mass counterterm. Operator $O_{t\phi}$ does not have a physical effect in this process, as it only shifts the top-quark mass which is an input parameter. Therefore it is equivalent to redefine $O_{t\phi}$ as $y_t^3 (\phi^\dagger \phi - v^2/2)(\bar{Q} t)\tilde{\phi}$, and shift the renormalization of the dimension-four component of $O_{t\phi}$, i.e. $-m_t^2/\Lambda^2 y_t (\bar{Q} t)\tilde{\phi}$, to Eq. (6). This is more convenient since $O_{t\phi}$ then completely drops out from the calculation.

Our calculation is performed using the MadGraph5_aMC@NLO framework [38]. The operator O_{tG} is implemented in the UFO format [43] by using the FeynRules package [44]. Helicity amplitude routines are generated by ALOHA [45]. The evaluation of the loop corrections requires two additional pieces, the UV counterterms and the rational R2 terms which are required by the Ossola-Papadopoulos-Pittau technique [46]. The UV counterterms are computed according to Eqs. (5)–(10), while the R2 terms are generated by the NLOCT package [47]. The calculation is then automatically performed by MadGraph5_aMC@NLO at NLO accuracy, and matched to parton shower via the MC@NLO formalism [48].

Several checks of the implementation have been done, including the gauge invariance of all virtual contributions, and the pole cancellation when combining virtual and real contributions. In addition, we checked that all relevant UV and R2 terms are correctly implemented, by computing individual diagrams with MadLoop [49] and comparing with analytical results obtained by using FormCalc and LoopTools [50].

IV. TOTAL CROSS SECTION

In this section we give the NLO total cross section from O_{tG}, and place limits on its size, using available measurements from the Tevatron and the LHC.

As mentioned above, we work up to $\mathcal{O}(\Lambda^{-2})$, which means we insert in each diagram at most one effective vertex from O_{tG}. The total cross section then becomes a quadratic function of C_{tG}/Λ^2,

$$\sigma = \sigma_{\rm SM} + \frac{C_{tG}}{\Lambda^2}\beta_1 + \left(\frac{C_{tG}}{\Lambda^2}\right)^2 \beta_2. \tag{11}$$

The β_1 term represents the contribution from O_{tG} at order $\mathcal{O}(\Lambda^{-2})$. The quadratic β_2 term, on the other hand, does not have a physical meaning without a complete calculation at $\mathcal{O}(\Lambda^{-4})$, and needs to be dropped. However the size of this term can be used to gauge the range in which the approach itself is valid, or in other words, the expansion in $1/\Lambda$ converges.

To extract $\beta_{1,2}$, we perform the calculation with C_{tG} taking different values: $0, \pm 1, \pm 2$, and fit the resulting cross sections to Eq. (11). Each run is performed with 9 combinations of (μ_R,μ_F), where μ_R is the renormalization scale and μ_F the factorization scale, each can take values $\mu/2, \mu$ and 2μ, with the central value $\mu = m_t$. This allows us to extract the scale variation of β_1. In our calculation $m_t = 173.3$ GeV, and we use the NNPDF 2.3 set of the parton distribution functions [51]. The values of $\beta_{1,2}$, both at LO and NLO, are given in Table I for Tevatron, LHC 8 TeV, LHC 13 TeV and LHC 14 TeV runs. A significant improvement in the scale dependence can be noticed. A large K factor is found at the LHC. The sizes of β_2 imply that the effective approach is valid given that $C_{tG}/\Lambda^2 \lesssim 1$ TeV^{-2}. Our LO results agree with Ref. [52] once we take into account scale variation and note the opposite sign convention of d_V.

With these results we can set bounds on the size of O_{tG} using total cross section measurements. We replace the $\sigma_{\rm SM}$ in Eq. (11) by the most precise SM predictions at NNLO + NNLL accuracy in QCD, which are $\sigma_{\rm SM}^{\rm TeV} = 7.148 \pm 0.218$ pb and $\sigma_{\rm SM}^{\rm LHC} = 244.9 \pm 9.7$ pb respectively for Tevatron and for LHC at 8 TeV [53]. We sum the scale and parton distribution function uncertainties in quadrature and symmetrize the error around a central value. The combined measurement at the Tevatron (LHC) is $\sigma_{\rm exp}^{\rm TeV} = 7.51 \pm 0.40$ pb ($\sigma_{\rm exp}^{\rm LHC} = 240.6 \pm 8.5$ pb) [54,55], where we have corrected for the top-mass difference using the prescription given in these references. The value of C_{tG} can be extracted using

$$\frac{C_{tG}}{\Lambda^2} = \frac{\sigma_{\rm exp} - \sigma_{\rm SM}}{\beta_1}, \tag{12}$$

together with its corresponding uncertainty, given by

$$\frac{\delta C_{tG}}{\Lambda^2} = \left|\frac{\sigma_{\rm exp} - \sigma_{\rm SM}}{\beta_1}\right| \left[\frac{\epsilon_{\rm exp}^2 + \epsilon_{\rm SM}^2}{(\sigma_{\rm exp} - \sigma_{\rm SM})^2} + \left(\frac{\epsilon_{\beta_1}}{\beta_1}\right)^2\right]^{\frac{1}{2}} \tag{13}$$

where the experimental error $\epsilon_{\rm exp}$ and the theoretical NNLO error $\epsilon_{\rm SM}$ are summed in quadrature, and ϵ_{β_1} is the (symmetrized) error of β_1 due to scale variations. We assume no correlation between the SM NNLO prediction and β_1. One could also add in Eq. (13) a term representing the error from the missing $\mathcal{O}(\Lambda^{-4})$ terms, which can be

TABLE I. Values of β_1 and β_2 at LO and NLO precisions for the Tevatron, and for the LHC at 8, 13, and 14 TeV. The respective K factors for the central values of β_1 are also shown.

β_1	LO [pb TeV^2]	NLO [pb TeV^2]	K factor
Tevatron	$1.61^{+0.66\ (+41\%)}_{-0.43\ (-27\%)}$	$1.810^{+0.073\ (+4.05\%)}_{-0.197\ (-10.88\%)}$	1.12
LHC8	$50.7^{+17.3\ (+34\%)}_{-12.4\ (-25\%)}$	$72.62^{+9.26\ (+12.7\%)}_{-10.53\ (-14.5\%)}$	1.43
LHC13	$161.6^{+48.0\ (+29.7\%)}_{-36.2\ (-22.4\%)}$	$239.5^{+29.0\ (+12.1\%)}_{-31.8\ (-13.3\%)}$	1.48
LHC14	$191.3^{+55.6\ (+29.0\%)}_{-42.2\ (-22.0\%)}$	$283.0^{+33.6\ (+11.9\%)}_{-36.9\ (-13.1\%)}$	1.48

β_2	LO [pb TeV^4]	NLO [pb TeV^4]
Tevatron	0.156	0.158
LHC8	8.94	11.8
LHC13	30.0	43.2
LHC14	35.7	51.6

TABLE II. Limits on C_{tG}/Λ^2. The corresponding limits combining Tevatron and LHC8, in terms of d_V, is $[-0.0099, 0.0123]$ at LO and $[-0.0096, 0.0090]$ at NLO (note the opposite sign convention of d_V in [52]). For LHC14 we assume a 5% experimental error.

	LO [TeV^{-2}]	NLO [TeV^{-2}]
Tevatron	[−0.33, 0.75]	[−0.32, 0.73]
LHC8	[−0.56, 0.41]	[−0.42, 0.30]
LHC14	[−0.56, 0.61]	[−0.39, 0.43]

estimated using $\beta_2(C_{tG}/\Lambda^2)^2$, but the changes in the limits are negligible.

We show the 95% CL allowed region for C_{tG} in Table II. The improvement of NLO calculation for Tevatron is mild due to the small K factor. In the LHC cases the allowed range is significantly reduced at NLO. We also give the expected limit at the LHC 14 TeV run, assuming an experimental error of $\pm 5\%$.

V. DISTRIBUTIONS

Our calculation is implemented via the MadGraph5_aMC@NLO framework, therefore simulation of any observable is automatic. In this section we present a few representative distributions of variables of particular relevance for LHC phenomenology. To simulate parton shower we have used the Herwig 6 code [56]. Other shower programs are also available, including Herwig $++$ [57] and Pythia 8 [58].

A. Stable top quarks

We first look at kinematic observables constructed from stable top-quark pairs. In Fig. 3 and Fig. 4 we show the invariant mass of the top antitop system and the transverse momentum of the top quark for the LHC at 8 TeV, in each case with the differential K factor displayed in the lower panel. The contribution from O_{tG} is extracted by generating event samples with $C_{tG} = \pm 2$ separately and taking the difference, in order to get rid of the quadratic terms in C_{tG}. These observables can serve as discriminators in case any deviation from the SM is observed, and will be useful in determining the type of new physics [37]. One can see that the NLO computation reduces the scale variation. The differential K factor is not a constant and drops at higher scales; however, in both distributions we observe that the K factor of the O_{tG} contribution is similar to that of the SM

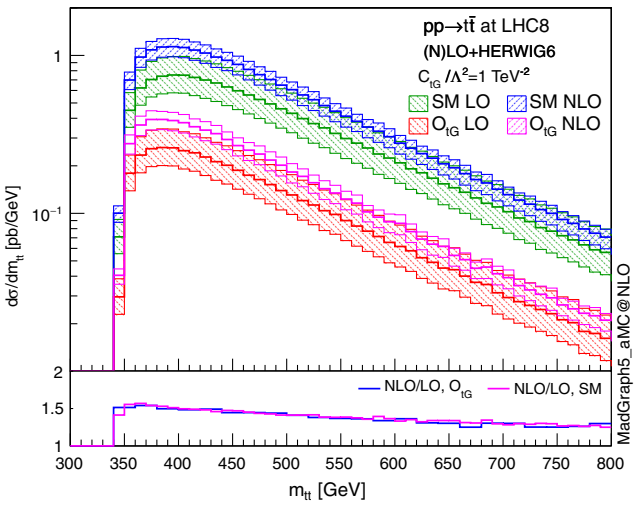

FIG. 3 (color online). Top-quark pair invariant mass distribution at LHC 8 TeV.

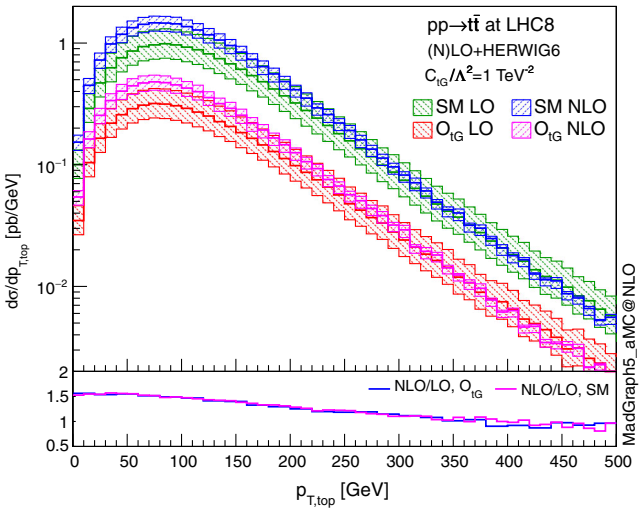

FIG. 4 (color online). Top-quark transverse momentum distribution at LHC 8 TeV.

contribution, so using the SM K factor to rescale the LO event samples from O_{tG} can be a good approximation of the complete NLO result. Note that we have chosen $C_{tG}/\Lambda^2 = 1\ \text{TeV}^{-2}$ for convenience, even though this value is already excluded by the current limits. One can always rescale the curve to get corresponding result for any other value of C_{tG}, as we have already removed the quadratic dependence on C_{tG}.

In Fig. 5 we show the top-quark pair invariant mass distribution for LHC at 14 TeV, at high mass region above 1 TeV. In this calculation we have set $\mu = 1$ TeV. It has been suggested that the O_{tG} operator can be more easily accessed at large $t\bar{t}$ invariant masses, for instance in the

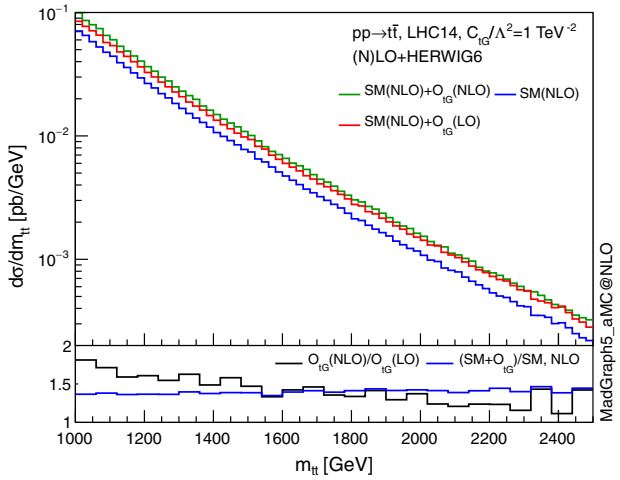

FIG. 5 (color online). Top-quark pair invariant mass distribution above 1 TeV, at the LHC 14 TeV energy. The renormalization and factorization scales are taken to be 1 TeV. The lower panel shows that the K factor for O_{tG} decreases at high mass region, and the signal over background ratio, $\sigma(O_{tG})/\sigma(\text{SM})$, is almost a constant.

top-quark angular distributions [27], in the total cross sections [52] and in boosted top analysis [59]. This is because higher momentum transfer is favored by the dipole structure of O_{tG}. However, using NLO (or NNLO) prediction for the SM together with only LO prediction for O_{tG} may lead us to overestimate this effect, because the K factor decreases at larger energy scales. From Fig. 5 we can see that the signal excess, $\sigma(O_{tG})/\sigma(\mathrm{SM})$, is flat at a large energy range. In fact, at order $\mathcal{O}(\Lambda^{-2})$, $\sigma(O_{tG})$ is suppressed by a constant factor of m_t^2/Λ^2 compared with $\sigma(\mathrm{SM})$, instead of s/Λ^2 or $\sqrt{s}m_t/\Lambda^2$ as one might have expected naively by power counting. This is because the Higgs field in O_{tG} always takes the vacuum expectation value, and the O_{tG} operator flips the chirality of the top quark in its interference with the SM amplitude. Including higher-order terms in $1/\Lambda^2$ can give rise to additional contributions that will indeed rise faster at large s, but if such an effect is large, it would imply the breakdown of the effective operator framework since the expansion in $1/\Lambda$ does not converge at large energy. In Table III we show K factors for SM and O_{tG} as well as $\sigma(O_{tG})/\sigma(\mathrm{SM})$, with no cuts and with cuts $m_{t\bar{t}} > 1$ TeV and 2 TeV. Both LO and NLO give similar results for the signal excess, but using LO prediction for O_{tG} with NLO for SM leads to an artificial rise at large $m_{t\bar{t}}$, due to the decreasing K factor of the SM.

Another interesting observable is the forward-backward asymmetry, A_{FB}, which has been observed at the Tevatron both by D0 [60] and CDF [61]. A_{FB} is defined as the asymmetry with respect to $\Delta y = y_t - y_{\bar{t}}$. In the SM the first nonzero contribution arises at NLO in QCD. In a dimension-six Lagrangian, only four-fermion operators can give a contribution at the tree level, and so A_{FB} is another important observable that distinguishes between different new physics scenarios. In this respect, it is useful to know the first nonvanishing contribution from the CMDM operator, which appears at NLO, to at least have some estimation of the corresponding theoretical uncertainty related to this quantity. In our framework this calculation is straightforward. We expand the numerator and the denominator of A_{FB} to NNLO for the SM part and NLO for the O_{tG} part, and we find

$$\begin{aligned} A_{FB} &= \frac{N_{\mathrm{EW}} + \alpha_s^3 N_3 + \alpha_s^4 N_4 + \alpha_s^3 \frac{C_{tG}}{\Lambda^2} N_{tG} + \mathcal{O}(\alpha_s^5, \alpha_s^4 \Lambda^{-2})}{\alpha_s^2 D_2 + \alpha_s^3 D_3 + \alpha_s^4 D_4 + \alpha_s^3 \frac{C_{tG}}{\Lambda^2} D_{tG} + \mathcal{O}(\alpha_s^5, \alpha_s^4 \Lambda^{-2})} \\ &= A_{FB}(\mathrm{SM}) + \frac{C_{tG}}{\Lambda^2} \frac{\alpha_s N_{tG}}{D_2} + \mathcal{O}(\alpha_s^3, \alpha_s^2 \Lambda^{-2}) \\ &= 0.095 \pm 0.007 + C_{tG} 0.021^{+0.003}_{-0.002} \left(\frac{\mathrm{TeV}}{\Lambda}\right)^2 \end{aligned} \tag{14}$$

where the SM prediction at NNLO in QCD is taken from Ref. [62], and the uncertainties of the second term come from scale variation. We thus expect a small modification to A_{FB} from a nonvanishing CMDM. Given the current limit on C_{tG}, however, this contribution is much smaller than the experiment uncertainties.

Once differential cross sections are known, one can consider constraining the CMDM by using the normalized distributions of the $t\bar{t}$ observables. Unfortunately from Fig. 3 and Fig. 4 one can see that the shapes of the distributions from O_{tG} are not significantly different than those from the SM. As a result the limits obtained only by using the shape of the distribution will be loose. As an example we consider the $t\bar{t}$ invariant mass distribution at 7 TeV measured by the CMS Collaboration [63]. We take only the first four bins, i.e. from 345 to 650 GeV, to ensure the validity of the expansion in $1/\Lambda^2$ for Λ around TeV scale. We perform a simple χ^2 fit for the differential cross section normalized within these four bins. We add the experimental and theoretical errors in quadrature. The SM prediction is computed with MadGraph5_aMC@NLO and then normalized to the most accurate NNLO + NNLL prediction [53], with uncertainties coming from the renormalization and factorization scale variation. The 95% CL allowed region is [−5.0,12.8], using LO predictions for the O_{tG} contribution, and [−0.6,10.9] when using NLO prediction. Despite a significant improvement at NLO, the limit itself is much looser than those obtained from total cross sections; therefore, we expect only a small improvement when the distribution information is combined together with the total cross section in such analyses.

TABLE III. K factor and signal excess $\sigma(O_{tG})/\sigma(\mathrm{SM})$, with no cuts, and with cuts $m_{t\bar{t}} > 1$ TeV and 2 TeV. $\mu = m_t$. Both LO and NLO give similar results for the signal excess, but using LO prediction for O_{tG} and NLO for SM leads to an artificial rise at large $m_{t\bar{t}}$.

	No cuts	$m_{t\bar{t}} > 1$ TeV	$m_{t\bar{t}} > 2$ TeV
K (SM)	1.49	1.16	0.77
K (O_{tG})	1.49	1.14	0.69
O_{tG}(LO)/SM(LO)	0.32	0.28	0.29
O_{tG}(NLO)/SM(NLO)	0.32	0.28	0.26
O_{tG}(LO)/SM(NLO)	0.21	0.24	0.37

B. Decayed top quarks

The above results indicate that the kinematic observables constructed from stable $t\bar{t}$ system are not very sensitive to the size of the top-quark CMDM. We therefore move on to include top-quark decays, where we expect that the decay products preserve the spin information of the top quarks, and thus can be more sensitive to the dipole structure in the operator. As an example we focus on the dimuon channel, where both top quarks decay semileptonically into a b-quark and a muon. We use the MadSpin package [39] to decay the top quarks, so that the spin correlation at LO accuracy is preserved in the simulation.

In our simulation we use the anti-k_T algorithm for the jets with radius $R = 0.5$. The following cuts are imposed to

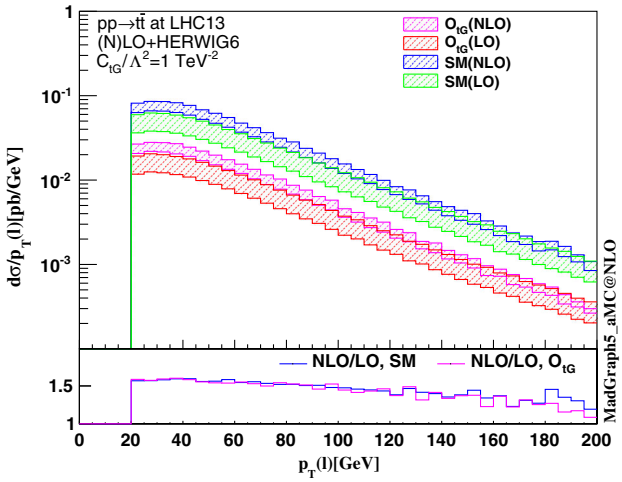

FIG. 6 (color online). Transverse momentum distribution of the hardest muon at LHC 13 TeV.

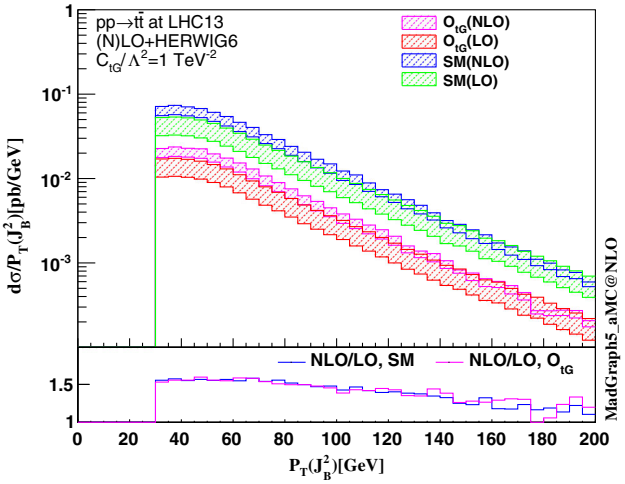

FIG. 8 (color online). Transverse momentum distribution of the second hardest b-jet at LHC 13 TeV.

mimic the environment of a real detector: $p_T(j) > 30$ GeV, $|\eta(j)| < 2.5$, $p_T(\ell) > 20$ GeV and $\eta(\ell)| < 2.5$, where j refers to jets and ℓ to muons. At least two jets, from which at least one containing a b-hadron, and exactly one pair of isolated muons are required. The isolation criteria is achieved by imposing a maximum value of 0.15 on the ratio of the scalar sum of p_T of all hadronic tracks within $\Delta R = \sqrt{\Delta\eta^2 + \Delta\phi^2} < 0.3$ around the muon candidate, to the transverse momentum of the muon. We show in Fig. 6 the transverse momentum distribution of the muon. In Figs. 7–8 we show the hardest (largest p_T) and the second hardest (when present in the event) b-jets, respectively. In Fig. 9 the azimuthal angle difference between the two selected muons is shown.

This last distribution is particularly important for the measurement of the O_{tG} operator, because it is sensitive to the spin correlation between the top quarks. The anomalous top-quark CMDM affects the spin correlation of the $t\bar{t}$ system [27,64], and its effects have been searched for by the CMS Collaboration [29]. The contribution from the O_{tG} operator to this distribution, expanded linearly in C_{tG}, takes the following form:

$$\left(\frac{1}{\sigma}\frac{d\sigma}{d|\Delta\phi|}\right) = \left(\frac{1}{\sigma}\frac{d\sigma}{d|\Delta\phi|}\right)_{\rm SM} + \frac{C_{tG}}{\Lambda^2}\left(\frac{1}{\sigma}\frac{d\sigma}{d|\Delta\phi|}\right)_{\rm NP} \quad (15)$$

which is valid provided $C_{tG}\beta_1/\Lambda^2 \ll \sigma_{\rm SM}$. In the spirit of perturbation theory, the second term on the rhs of Eq. (15) can be expanded to $\mathcal{O}(\alpha_S)$:

$$\left(\frac{1}{\sigma}\frac{d\sigma}{d|\Delta\phi|}\right)^{\rm NLO}_{\rm NP} = \left(\frac{1}{\sigma}\frac{d\sigma}{d|\Delta\phi|}\right)^{\rm LO}_{\rm NP} + \left(\frac{1}{\sigma}\frac{d\sigma}{d|\Delta\phi|}\right)^{(1)}_{\rm NP} \quad (16)$$

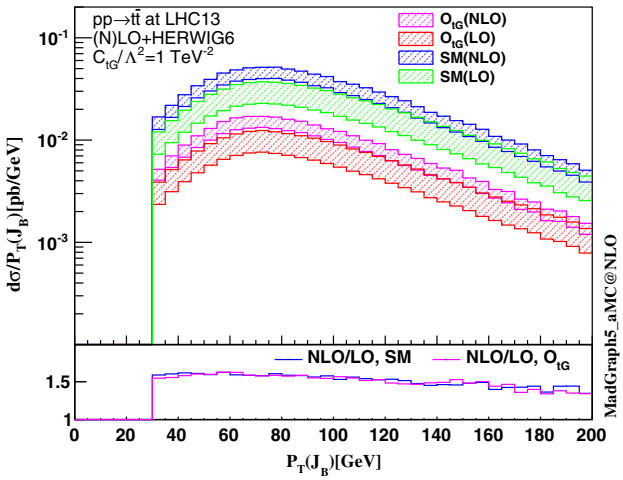

FIG. 7 (color online). Transverse momentum distribution of the hardest b-jet at LHC 13 TeV.

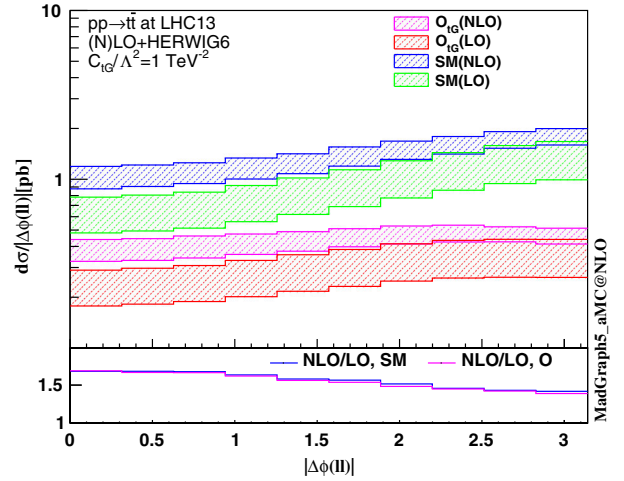

FIG. 9 (color online). Difference in azimuthal angle between the two selected muons at LHC 13 TeV. Note that the K factor changes in a way that enhances the deviation of the O_{tG} contribution from the SM.

where

$$\left(\frac{1}{\sigma}\frac{d\sigma}{d|\Delta\phi|}\right)^{\rm LO}_{\rm NP} = \frac{1}{\sigma^{\rm LO}_{\rm SM}}\left(\frac{d\sigma^{\rm LO}_{O_{tG}}}{d|\Delta\phi|}\right) - \frac{\beta^{\rm LO}_1}{\sigma^{\rm LO\,2}_{\rm SM}}\left(\frac{d\sigma^{\rm LO}_{\rm SM}}{d|\Delta\phi|}\right) \quad (17)$$

and

$$\left(\frac{1}{\sigma}\frac{d\sigma}{d|\Delta\phi|}\right)^{(1)}_{\rm NP} = \frac{1}{\sigma^{\rm LO}_{\rm SM}}\left(\frac{d\sigma^{(1)}_{O_{tG}}}{d|\Delta\phi|}\right) - \frac{1}{\sigma^{\rm LO\,2}_{\rm SM}}\left[\beta^{(1)}_1\left(\frac{d\sigma^{\rm LO}_{\rm SM}}{d|\Delta\phi|}\right) + \beta^{\rm LO}_1\left(\frac{d\sigma^{(1)}_{\rm SM}}{d|\Delta\phi|}\right) + \sigma^{(1)}_{\rm SM}\left(\frac{d\sigma^{\rm LO}_{O_{tG}}}{d|\Delta\phi|}\right)\right] + \frac{2\sigma^{(1)}_{\rm SM}\beta^{\rm LO}_1}{\sigma^{\rm LO\,3}_{\rm SM}}\left(\frac{d\sigma^{\rm LO}_{\rm SM}}{d|\Delta\phi|}\right) \quad (18)$$

where $d\sigma_{O_{tG}}$ represents the distribution from operator O_{tG} for $C_{tG}/\Lambda^2 = 1$ TeV^{-2}. The superscript (1) indicates the α_S correction to the corresponding LO quantity.

The predicted distribution is shown in Fig. 10 for $C_{tG}/\Lambda^2 = 1$ TeV^{-2}. The O_{tG} contribution has a peculiar structure which tends to flatten the distribution. In Fig. 11 we show the O_{tG} distributions solely, as defined in Eqs. (16)–(18). The first observation is that the purple and the red curves are very close to each other, indicating that the LO and NLO results are very similar. The reason is that we are plotting the normalized distribution, and since the K factors are almost the same for the SM and for the O_{tG}, they cancel each other when taking the ratio. In fact, one can see that Eq. (17) vanishes if the K factor is a constant. Alternatively, if we use NLO prediction for the SM but only LO prediction for O_{tG}, following the logic that the radiative correction on the new physics effect is of higher order, then we will have

$$\left(\frac{1}{\sigma}\frac{d\sigma}{d|\Delta\phi|}\right)^{\rm nlo}_{\rm NP} = \frac{1}{\sigma^{\rm NLO}_{\rm SM}}\left(\frac{d\sigma^{\rm LO}_{O_{tG}}}{d|\Delta\phi|}\right) - \frac{\beta^{\rm LO}_1}{\sigma^{\rm NLO\,2}_{\rm SM}}\left(\frac{d\sigma^{\rm LO}_{\rm SM}}{d|\Delta\phi|}\right). \quad (19)$$

This result, after expanding in α_s, contains only part of the $\mathcal{O}(\alpha_s\Lambda^{-2})$ corrections in Eq. (18) (and so we refer to as "nlo"). They come from the $\mathcal{O}(\alpha_s)$ corrections to the normalization, but not directly to the O_{tG} contribution. The missing $\mathcal{O}(\alpha_s\Lambda^{-2})$ terms actually make a large difference, as illustrated by the blue curve in Fig. 11. One can see that Eq. (19) gives a much lower estimation for the effect of O_{tG}. This is not only because of the overall size of the K factor, but also due to the fact that the K factor is a decreasing function of $\Delta\phi(ll)$, and so the way it changes adds coherently to the difference in shapes between O_{tG} and SM distributions, as can be seen in Fig. 9. As a result, using NLO prediction for the SM together with only LO prediction for O_{tG} significantly underestimates the power of $\Delta\phi(ll)$ in discriminating the O_{tG} contribution from the SM. Also note that, the fact that Eq. (19) and the LO prediction in Eq. (17) differ implies that the LO prediction for O_{tG} has a large uncertainty due to the missing $\mathcal{O}(\alpha_s\Lambda^{-2})$ terms, which turn out to have a large effect in this special case. Thus our work improves the precision level of this prediction by completing the missing $\mathcal{O}(\alpha_s\Lambda^{-2})$ terms.

We also show for completeness two more angular distributions which have been studied by Ref. [27]. Following Ref. [27] we define $\vec{\ell}^-$ ($\vec{\ell}^+$) as the momenta of the (anti-)muon in the rest frame of antitop (top) quarks

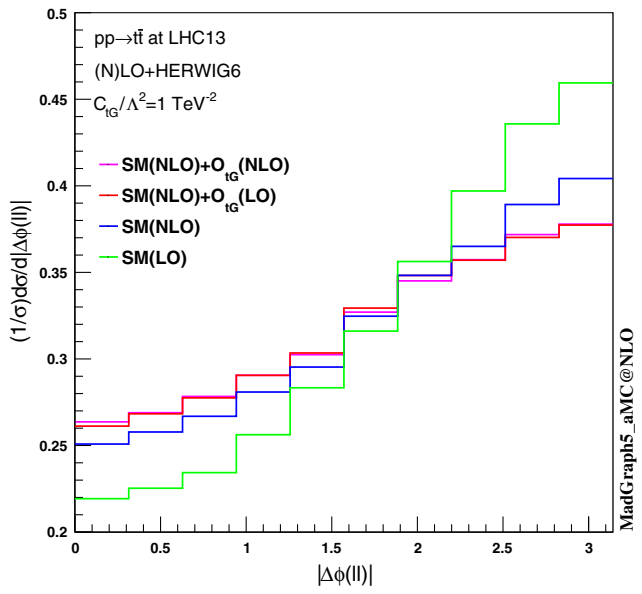

FIG. 10 (color online). Normalized distributions of the difference in azimuthal angle between muons.

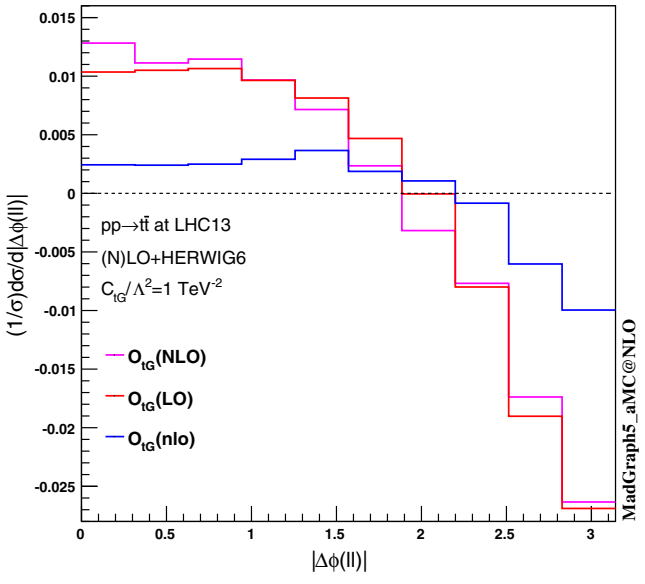

FIG. 11 (color online). New physics contribution to the normalized dimuon distribution at the LHC (13 TeV), $(\sigma^{-1}d\sigma/d|\Delta\phi|)_{NP}$ defined in Eqs. (15)–(19).

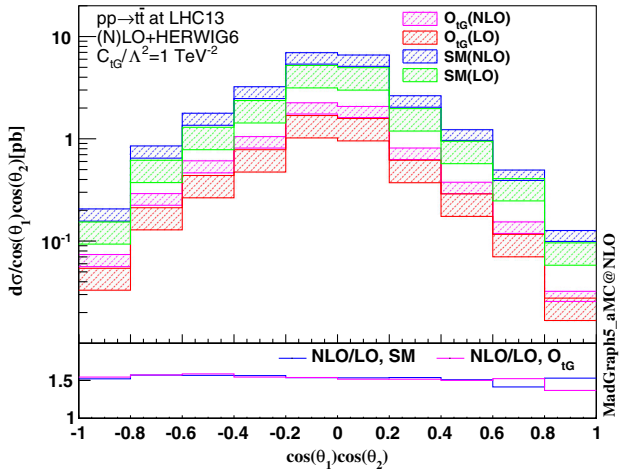

FIG. 12 (color online). $\cos\theta_1 \cos\theta_2$ distribution at LHC 13 TeV.

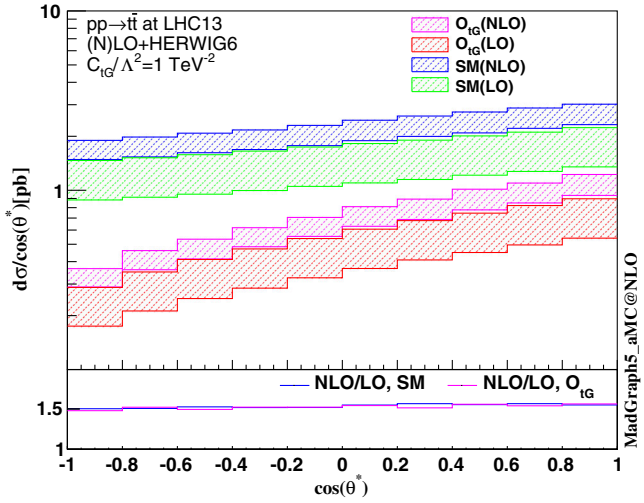

FIG. 13 (color online). $\cos\theta^*$ distribution at LHC 13 TeV.

and $\vec{k}$ ($\bar{\vec{k}}$) the momenta of the top (antitop) in the zero-momentum frame. In Fig. 12 we show the distribution of $\cos\theta_1 \cos\theta_2$, where θ_1 (θ_2) is the angle $\measuredangle(\vec{\ell}^-, \bar{\vec{k}})$ [$\measuredangle(\vec{\ell}^+, \vec{k})$]. In Fig. 13 we show the normalized distribution of $\cos\theta^*$, where θ^* is the angle $\measuredangle(\vec{\ell}^-, \vec{\ell}^+)$. Contrary to the $|\Delta\phi(\ell\ell)|$ case, where the QCD corrections enhances the anomalous coupling contribution to the shape, in these cases, we observe a uniform QCD correction with no effect in the normalized distributions.

VI. CONCLUSIONS

In this work we have presented the NLO calculation for top-quark pair production, including an anomalous top-quark CMDM, as described by the dimension-six operator O_{tG}. Our calculation is implemented in the MadGraph5_aMC@NLO framework, which allows the result to be matched to parton shower automatically. We have studied the impact of QCD corrections to the contribution of the CMDM in top-quark pair production, both on total cross section as well as on various distributions.

The QCD correction increases the overall contribution from the O_{tG} operator. For the total cross section for example, the increase is, at central scale, 12%, 43% and 48% for Tevatron, LHC8 and LHC14 respectively. Moreover, the NLO calculation significantly reduces the scale uncertainty of the contribution from O_{tG}. Limits on the coefficient of C_{tG} are therefore improved. Our predicted allowed range at 95% CL using Tevatron and LHC8 data is $-0.32 < C_{tG} < 0.30$ (assuming $\Lambda = 1$ TeV), which in terms of d_V parameter gives $-0.0096 < d_V < 0.0090$.

Our implementation can be used for various exclusive studies. We have shown representative distributions for both stable and decayed top quarks as examples. We observed a significant reduction of scale variation in all distributions. The differential K factor is not a constant, but for all observables we have studied, it is similar to the SM K factor. Therefore we expect that using the SM K factor to rescale the LO contribution of O_{tG} can be a good approximation for a NLO prediction in most cases. On the other hand, using NLO SM prediction together with LO prediction of O_{tG} can be misleading in analysis where the ratio between O_{tG} contribution and SM contribution can play a role. Observables sensitive to spin correlation can also be studied in the same framework, provided that the MadSpin package is used to preserve the spin information of the top quarks. This is particularly useful for spin correlation measurements where limits can be set by using various angular distributions of the decay products. We showed that the NLO correction does not significantly change the LO prediction, but instead it increases the precision level, in particular for the $\Delta\phi(ll)$ distribution, where using NLO SM prediction together with LO prediction of O_{tG} can lead us to underestimate the effect from top-quark CMDM.

Our theoretical approach is based on the effective field theory for top-quark couplings, and is a first step of the automation of the top-quark flavor-diagonal operators in the MadGraph5_aMC@NLO framework. The next step is to extend our study to other top-quark operators, including the CP-odd ones such as the CEDM, as well as other electroweak couplings of the top quark. These studies will pave the way to a global analysis for top-quark couplings using the effective field theory framework.

ACKNOWLEDGMENTS

We would like to thank C. Degrande, V. Hirschi, F. Maltoni and M. Zaro for many helpful discussions and patient explanations. C. Z. is supported by U.S. Department of Energy under Grant No. DE-AC02-98CH10886. D. B. F. is supported by the Danish National Research Foundation, Grant No. DNRF90.

[1] K. Olive *et al.* (Particle Data Group), Review of particle physics, Chin. Phys. C **38**, 090001 (2014).

[2] J. Drobnak, S. Fajfer, and J. F. Kamenik, QCD corrections to flavor changing neutral coupling mediated rare top quark decays, Phys. Rev. D **82**, 073016 (2010).

[3] J. Drobnak, S. Fajfer, and J. F. Kamenik, Flavor Changing Neutral Coupling Mediated Radiative Top Quark Decays at Next-to-Leading Order in QCD, Phys. Rev. Lett. **104**, 252001 (2010).

[4] C. Zhang and F. Maltoni, Top-quark decay into Higgs boson and a light quark at next-to-leading order in QCD, Phys. Rev. D **88**, 054005 (2013).

[5] J. Drobnak, S. Fajfer, and J. F. Kamenik, New physics in $t \to bW$ decay at next-to-leading order in QCD, Phys. Rev. D **82**, 114008 (2010).

[6] C. Zhang, Effective field theory approach to top-quark decay at next-to-leading order in QCD, Phys. Rev. D **90**, 014008 (2014).

[7] J. J. Liu, C. S. Li, L. L. Yang, and L. G. Jin, Next-to-leading order QCD corrections to the direct top quark production via model-independent FCNC couplings at hadron colliders, Phys. Rev. D **72**, 074018 (2005).

[8] J. Gao, C. S. Li, J. J. Zhang, and H. X. Zhu, Next-to-leading order QCD corrections to the single top quark production via model-independent tqg flavor-changing neutral-current couplings at hadron colliders, Phys. Rev. D **80**, 114017 (2009).

[9] Y. Zhang, B. H. Li, C. S. Li, J. Gao, and H. X. Zhu, Next-to-leading order QCD corrections to the top quark associated with γ production via model-independent flavor-changing neutral-current couplings at hadron colliders, Phys. Rev. D **83**, 094003 (2011).

[10] B. H. Li, Y. Zhang, C. S. Li, J. Gao, and H. X. Zhu, Next-to-leading order QCD corrections to tZ associated production via the flavor-changing neutral-current couplings at hadron colliders, Phys. Rev. D **83**, 114049 (2011).

[11] Y. Wang, F. P. Huang, C. S. Li, B. H. Li, D. Y. Shao, and J. Wang, Constraints on flavor-changing neutral-current Htq couplings from the signal of tH associated production with QCD next-to-leading order accuracy at the LHC, Phys. Rev. D **86**, 094014 (2012).

[12] D. Y. Shao, C. S. Li, J. Wang, J. Gao, H. Zhang, and H. X. Zhu*et al.*, Model independent analysis of top quark forward-backward asymmetry at the Tevatron up to $\mathcal{O}(\alpha_s^2/\Lambda^2)$, Phys. Rev. D **84**, 054016 (2011).

[13] C. Degrande, F. Maltoni, J. Wang, and C. Zhang, Automatic computations at next-to-leading order in QCD for top-quark flavor-changing neutral processes, Phys. Rev. D **91**, 034024 (2015).

[14] R. Röntsch and M. Schulze, Constraining couplings of top quarks to the Z boson in $t\bar{t} + \mathrm{Z}$ production at the LHC, J. High Energy Phys. 07 (2014) 091.

[15] R. Röntsch and M. Schulze, Probing top-Z dipole moments at the LHC and ILC, arXiv:1501.05939.

[16] A. Stange and S. Willenbrock, Yukawa correction to top quark production at the Tevatron, Phys. Rev. D **48**, 2054 (1993).

[17] C.-S. Li, B.-Q. Hu, J.-M. Yang, and C.-G. Hu, Supersymmetric QCD corrections to top quark production in $p\bar{p}$ collisions, Phys. Rev. D **52**, 5014 (1995).

[18] J.-M. Yang and C.-S. Li, Supersymmetric electroweak corrections to top quark production at the Fermilab Tevatron, Phys. Rev. D **52**, 1541 (1995).

[19] J. M. Yang and C. S. Li, Top squark mixing effects in the supersymmetric electroweak corrections to top quark production at the Tevatron, Phys. Rev. D **54**, 4380 (1996).

[20] R. Martinez and J. A. Rodriguez, Anomalous chromomagnetic dipole moment of the top quark in the standard model and beyond, Phys. Rev. D **65**, 057301 (2002).

[21] D. Atwood, A. Kagan, and T. Rizzo, Constraining anomalous top quark couplings at the Tevatron, Phys. Rev. D **52**, 6264 (1995).

[22] R. Martinez, M. Perez, and N. Poveda, Chromomagnetic dipole moment of the top quark revisited, Eur. Phys. J. C **53**, 221 (2008).

[23] Z. Hioki and K. Ohkuma, Search for anomalous top-gluon couplings at LHC revisited, Eur. Phys. J. C **65**, 127 (2010).

[24] Z. Hioki and K. Ohkuma, Addendum to: Search for anomalous top-gluon couplings at LHC revisited, Eur. Phys. J. C **71**, 1535 (2011).

[25] Z. Hioki and K. Ohkuma, Latest constraint on nonstandard top-gluon couplings at hadron colliders and its future prospect, Phys. Rev. D **88**, 017503 (2013).

[26] J. F. Kamenik, M. Papucci, and A. Weiler, Constraining the dipole moments of the top quark, Phys. Rev. D **85**, 071501(R) (2012); **88**, 039903(E) (2013).

[27] W. Bernreuther and Z.-G. Si, Top quark spin correlations and polarization at the LHC: Standard model predictions and effects of anomalous top chromo moments, Phys. Lett. B **725**, 115 (2013).

[28] S. Chatrchyan *et al.* (CMS Collaboration), Measurements of $t\bar{t}$ Spin Correlations and Top-Quark Polarization Using Dilepton Final States in pp Collisions at $\sqrt{s} = 7$ TeV, Phys. Rev. Lett. **112**, 182001 (2014).

[29] S. Chatrchyan *et al.* (CMS Collaboration), Report No. CMS-PAS-TOP-14-005.

[30] P. L. Cho and E. H. Simmons, Searching for G3 in $t\bar{t}$ production, Phys. Rev. D **51**, 2360 (1995).

[31] T. G. Rizzo, Single top quark production as a probe for anomalous moments at hadron colliders, Phys. Rev. D **53**, 6218 (1996).

[32] C. Degrande, J. Gerard, C. Grojean, F. Maltoni, and G. Servant, Probing top-Higgs non-standard interactions at the LHC, J. High Energy Phys. 07 (2012) 036; J. High Energy Phys. 03 (2013) 032.

[33] L. Labun and J. Rafelski, Higgs two-gluon decay and the top-quark chromomagnetic moment, arXiv:1210.3150.

[34] K.-m. Cheung, Probing the chromoelectric and chromomagnetic dipole moments of the top quark at hadronic colliders, Phys. Rev. D **53**, 3604 (1996).

[35] P. Haberl, O. Nachtmann, and A. Wilch, Top-quark production in hadron-hadron collisions and anomalous top-quark–gluon couplings, Phys. Rev. D **53**, 4875 (1996).

[36] C. Zhang and S. Willenbrock, Effective-field-theory approach to top-quark production and decay, Phys. Rev. D **83**, 034006 (2011).

[37] C. Degrande, J.-M. Gerard, C. Grojean, F. Maltoni, and G. Servant, Non-resonant new physics in top pair production at hadron colliders, J. High Energy Phys. 03 (2011) 125.

[38] J. Alwall, R. Frederix, S. Frixione, V. Hirschi, F. Maltoni, O. Mattelaer, H.-S. Shao, T. Stelzer, P. Torrielli, and M. Zaro, The automated computation of tree-level and next-to-leading order differential cross sections, and their matching to parton shower simulations, J. High Energy Phys. 07 (2014) 079.

[39] P. Artoisenet, R. Frederix, O. Mattelaer, and R. Rietkerk, Automatic spin-entangled decays of heavy resonances in Monte Carlo simulations, J. High Energy Phys. 03 (2013) 015.

[40] R. Alonso, E. E. Jenkins, A. V. Manohar, and M. Trott, Renormalization group evolution of the standard model dimension six operators III: Gauge coupling dependence and phenomenology, J. High Energy Phys. 04 (2014) 159.

[41] G. Durieux, F. Maltoni, and C. Zhang, A global approach to top-quark flavor-changing interactions, Phys. Rev. D **91**, 074017 (2015).

[42] J. C. Collins, F. Wilczek, and A. Zee, Low-energy manifestations of heavy particles: Application to the neutral current, Phys. Rev. D **18**, 242 (1978).

[43] C. Degrande, C. Duhr, B. Fuks, D. Grellscheid, O. Mattelaer, and T. Reiter, UFO: The universal FeynRules output, Comput. Phys. Commun. **183**, 1201 (2012).

[44] A. Alloul, N. D. Christensen, C. Degrande, C. Duhr, and B. Fuks, FeynRules 2.0: A complete toolbox for tree-level phenomenology, Comput. Phys. Commun. **185**, 2250 (2014).

[45] P. de Aquino, W. Link, F. Maltoni, O. Mattelaer, and T. Stelzer, ALOHA: Automatic libraries of helicity amplitudes for Feynman diagram computations, Comput. Phys. Commun. **183**, 2254 (2012).

[46] G. Ossola, C. G. Papadopoulos, and R. Pittau, Reducing full one-loop amplitudes to scalar integrals at the integrand level, Nucl. Phys. **B763**, 147 (2007).

[47] C. Degrande, Automatic evaluation of UV and R2 terms for beyond the Standard Model Lagrangians: A proof-of-principle, arXiv:1406.3030.

[48] S. Frixione and B. R. Webber, Matching NLO QCD computations and parton shower simulations, J. High Energy Phys. 06 (2002) 029.

[49] V. Hirschi, R. Frederix, S. Frixione, M. V. Garzelli, F. Maltoni, and R. Pittau, Automation of one-loop QCD corrections, J. High Energy Phys. 05 (2011) 044.

[50] T. Hahn and M. Perez-Victoria, Automatized one-loop calculations in four and D dimensions, Comput. Phys. Commun. **118**, 153 (1999).

[51] R. D. Ball, V. Bertone, S. Carrazza, C. S. Deans, L. D. Debbio *et al.*, Parton distributions with LHC data, Nucl. Phys. **B867**, 244 (2013).

[52] J. A. Aguilar-Saavedra, B. Fuks, and M. L. Mangano, Pinning down top dipole moments with ultra-boosted tops, arXiv:1412.6654 [Phys. Rev. D (to be published)].

[53] M. Czakon, P. Fiedler, and A. Mitov, Total Top-Quark Pair-Production Cross Section at Hadron Colliders Through $O(\alpha_S^4)$, Phys. Rev. Lett. **110**, 252004 (2013).

[54] T. A. Aaltonen *et al.* (CDF Collaboration and D0 Collaboration), Combination of measurements of the top-quark pair production cross section from the Tevatron Collider, Phys. Rev. D **89**, 072001 (2014).

[55] S. Chatrchyan *et al.* (CMS Collaboration), Technical Report No. CMS-PAS-TOP-14-016, CERN, Geneva, 2014.

[56] G. Corcella, I. Knowles, G. Marchesini, S. Moretti, K. Odagiri, P. Richardson, M. H. Seymour, and B. R. Webber, HERWIG 6: An Event generator for hadron emission reactions with interfering gluons (including supersymmetric processes), J. High Energy Phys. 01 (2001) 010.

[57] J. Bellm, S. Gieseke, D. Grellscheid, A. Papaefstathiou, S. Platzer *et al.*, Herwig++ 2.7 release note, arXiv:1310.6877.

[58] T. Sjostrand, S. Mrenna, and P. Z. Skands, A brief introduction to PYTHIA 8.1, Comput. Phys. Commun. **178**, 852 (2008).

[59] C. Englert, D. Goncalves, and M. Spannowsky, Non-standard top substructure, Phys. Rev. D **89**, 074038 (2014).

[60] V. M. Abazov *et al.* (D0 Collaboration), Measurement of the forward-backward asymmetry in top quark-antiquark production in ppbar collisions using the lepton+jets channel, Phys. Rev. D **90**, 072011 (2014).

[61] T. Aaltonen *et al.* (CDF Collaboration), Measurement of the top quark forward-backward production asymmetry and its dependence on event kinematic properties, Phys. Rev. D **87**, 092002 (2013).

[62] M. Czakon, P. Fiedler, and A. Mitov, Resolving the Tevatron top quark forward-backward asymmetry puzzle, arXiv:1411.3007.

[63] S. Chatrchyan *et al.* (CMS Collaboration), Measurement of differential top-quark pair production cross sections in pp collisions at $\sqrt{s} = 7$ TeV, Eur. Phys. J. C **73**, 2339 (2013).

[64] S. S. Biswal, S. D. Rindani, and P. Sharma, Probing chromomagnetic and chromoelectric couplings of the top quark using its polarization in pair production at hadron colliders, Phys. Rev. D **88**, 074018 (2013).